

The use of ilmenite as oxygen carrier with kerosene in a 300 W CLC laboratory reactor with continuous circulation

Patrick Moldenhauer^{a,*}, Magnus Rydén^a, Tobias Mattisson^a, Mourad Younes^b, Anders Lyngfelt^a

^aChalmers University of Technology, Department of Energy and Environment, Division of Energy Technology, 412 96 Göteborg, Sweden

^bSaudi Aramco, Research and Development Center, 313 11 Dharan, Saudi Arabia

Abstract

An ilmenite oxygen carrier was tested in a laboratory scale chemical-looping reactor with a nominal thermal capacity of 300 W_{th}. Ilmenite is a mineral iron-titanium oxide, which has been used extensively as an oxygen carrier in chemical-looping combustion. Two different kinds of fuels were used, a sulfur-free kerosene and one kerosene that contained 0.57 mass-% sulfur. Both fuels were continuously evaporated and directly fed into the chemical-looping reactor. Experiments were conducted for 50 h with the sulfur-free kerosene and for 30 h with the sulfurous kerosene. CO₂ yields above 99 % were achieved with both types of fuel. A significant and lasting improvement in the oxygen carrier's reactivity was observed, presumably an effect of using sulfurous kerosene. No evidence of sulfur was found on the particles' surface.

Keywords: chemical-looping combustion (CLC), liquid fuel, kerosene, sulfur, ilmenite oxygen carrier, circulating fluidized bed (CFB), CO₂ sequestration

1. Introduction

Chemical-looping combustion (CLC) is a method of burning carbon-based fuels with inherent sequestration of CO₂. The sequestration does not require extra energy and the net produced heat in CLC is the same as in regular combustion with air.

In chemical-looping combustion research, the use of liquid fuels is scarce and works with gaseous and solid fuels are predominant. Recent reviews concerning developments, advancements and operational experience in chemical-looping have been provided by Hossain and de Lasa [1], by Fang et al. [2], by Lyngfelt [3] and by Adánez et al. [4]. Only a handful of articles have been published that focus on the use of liquid fuels in chemical-looping applications. Pimenidou et al. used waste cooking oil in a batch packed-bed reactor to produce a synthesis gas [5], and addition of calcined dolomite as CO₂ sorbent added to the bed material was investigated to capture CO₂ and increase the concentration of hydrogen [6]. Cao et al. gasified bitumen and asphalt in a separate pyrolysis unit before feeding the synthesis gas into a batch fluidized-bed reactor [7]. Forret et al. and Hoteit et al. conducted chemical-looping combustion experiments, where liquid fuel was injected into a batch fluidized-bed reactor with a nickel-based oxygen carrier. The investigated fuels included n-dodecane [8], a domestic fuel oil and a heavy fuel oil [9]. Mendiara et al. investigated reforming of tar with different oxygen carriers by feeding nitrogen saturated with toluene into a batch fixed-bed reactor [10]. The production of hydrogen

from pyrolysis oils in a batch packed bed reactor was investigated by Lea-Langton et al., who used waste lubricating oil [11] and two biomass pyrolysis oils [12], and Giannakeas et al., who used scrap tire pyrolysis oil [13]. Moldenhauer et al. conducted both reforming and combustion experiments of sulfur-free kerosene in a fluidized-bed reactor with continuous circulation of oxygen carrier using nickel-based, copper-based and manganese-based oxygen carriers [14, 15]. This study is part of a project with the final aim of utilizing heavy oil residues for production of heat and power. Since heavy oil residues contain a significant amount of sulfur it is important to investigate the influence of sulfur on the oxygen carrier material in an early stage of the project. This study focuses on the influence of sulfur in kerosene on a mineral ilmenite oxygen carrier. The experiments were conducted in a laboratory scale chemical-looping reactor with two interconnected fluidized beds.

2. Experimental Details

2.1. 300 W Laboratory Reactor

The 300W chemical-looping reactor is a laboratory unit designed for testing oxygen carriers under continuous circulation of particles and with continuous fuel feed. It should not be seen as a pilot plant suitable for upscaling.

An illustration of the reactor, which was used in this work, is shown in Figure 1. The injection system for the liquid fuel, which is not visible in Figure 1, is connected to the inlet of the fuel reactor.

The reactor is 300 mm high. The fuel reactor has a cross-section of 25 mm × 25 mm. The base of the air reactor is 25 mm × 42 mm and contracts to 25 mm × 25 mm in the riser section.

*Corresponding author. Telephone: +46 (0)31-772 1469

Email address: patrick.moldenhauer@chalmers.se (Patrick Moldenhauer)

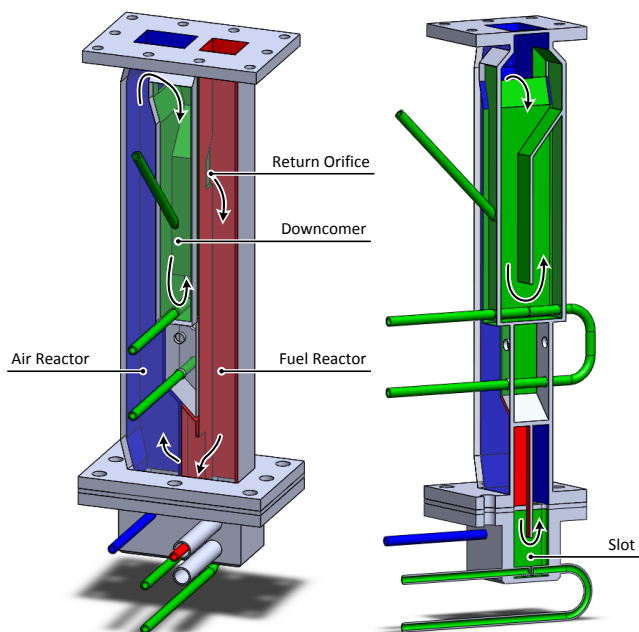
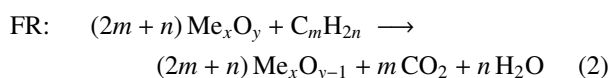
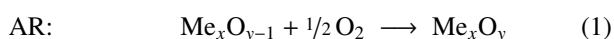


Figure 1: Schematic illustration of the 300 W chemical-looping reactor

Fuel and air enter the system through separate windboxes, located in the bottom of each reactor. Porous quartz plates act as gas distributors. In the air reactor, the gas velocity is sufficiently high to create a circulating fluidized-bed and oxygen carrier particles are thrown upwards. The particle-gas mixture is then separated: oxygen depleted air is returned to the atmosphere, whereas a fraction of particles falls into the standpipe of the downcomer, which is the inlet of a J-type loop-seal. From the loop-seal, particles overflow into the fuel reactor via the return orifice. The fuel reactor is a bubbling bed reactor. From the bottom of the fuel reactor, particles flow into the underflow standpipe of the slot, which is essentially a J-type loop-seal, and return to the air reactor, where the whole cycle starts over again.

The exit pipe of the fuel reactor is connected to a water seal with a column height of 1–2 cm. As a result, the pressure in the fuel reactor is 0.1–0.2 kPa higher than in the air reactor, which reduces gas leakage from air reactor to fuel reactor.

Metal oxide particles in the air reactor are fluidized with air, and reduced particles ($\text{Me}_x\text{O}_{y-1}$) are oxidized according to reaction (1). In the fuel reactor the metal particles are fluidized by gas-phase fuel or, in case of kerosene, a gaseous steam-fuel mixture. Particle reduction occurs by gas-phase fuel, according to reaction (2).



The 300 W reactor is subject to high heat losses due to a high surface-to-volume ratio. To achieve sufficiently high temperatures, typically 750–950°C, the reactor is encased in an electric furnace.

2.2. Injection Principle

The basic principle behind the injection system is to evaporate the liquid fuel using superheated steam as heat source and to inject the resulting steam-fuel gas mixture into the fuel reactor, see Figure 2. This is most convenient, because it causes the least changes to the reactor system, which is designed for gaseous fuels.

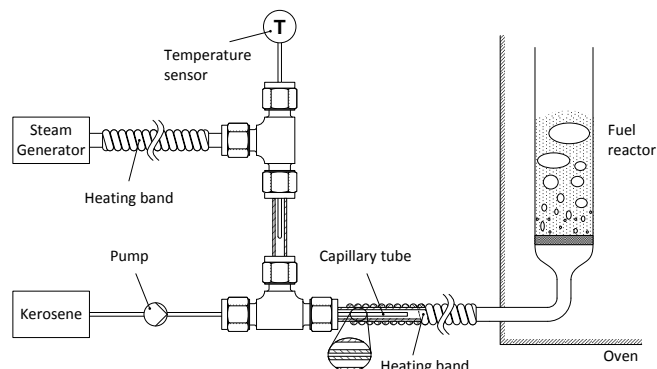


Figure 2: Schematic illustration of the injection system for kerosene injection

When the fuel molecules are converted the gas volume is increased. Hence, the volume flow of the gaseous steam-fuel mixture is a function of the extent of hydrocarbon converted. The steam fulfills the secondary function of ensuring that enough gas is available to fluidize the particles in the fuel reactor. Poorly fluidized particles increase the risk of agglomeration, which may destroy the oxygen carrier batch, depending upon the type of material used.

Figure 2 shows how evaporation, mixing and injection are realized. Steam is generated continuously by a steam generator. A heating band is used to superheat the steam to the desired temperature, which is measured by a thermocouple temperature sensor. A continuous fuel flow is provided by a diaphragm metering pump. The fuel is fed through a capillary tube, which is concentrically arranged within the steam pipe. The heat necessary for evaporation of the fuel is thereby transported from steam to fuel.

2.3. Fuel

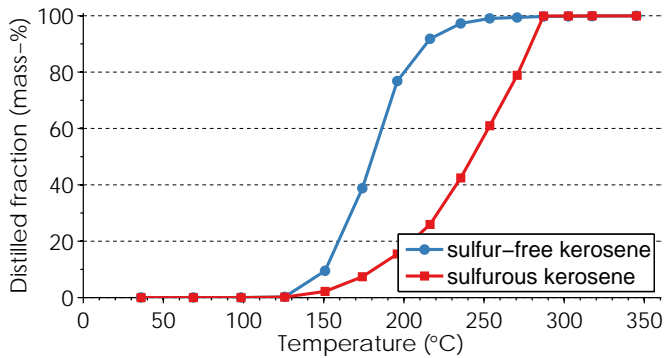
In this study, two similar types of fuels are used: sulfur-free kerosene and sulfurous kerosene. Both types were provided by courtesy of Preem AB in Gothenburg, Sweden. By definition, kerosene consists of different hydrocarbons with evaporation temperatures between 150°C and 320°C. The sulfur-free kerosene is produced through catalytic desulfurization of the sulfurous kerosene. Table 1 and Figure 3 show analyses of the two types of kerosene.

2.4. Oxygen Carrier

Ilmenite is a mineral that consists mainly of iron-titanium oxides (FeTiO_3) and some hematite (Fe_2O_3). To be used as an oxygen carrier, ilmenite is physically beneficiated and ground.

Table 1: Fuel analysis of sulfur-free and sulfurous kerosene

Fuel property	Sulfur-free kerosene	Sulfurous kerosene	Analysis method
C content (mass-%)	86.2 ± 0.5	85.9 ± 0.5	ASTM D 5291
H content (mass-%)	13.5 ± 0.4	13.5 ± 0.4	ASTM D 5291
N content (mass-%)	< 0.1 ± 0.03	< 0.1 ± 0.03	ASTM D 5291
S content (ppmw)	< 1	5700 ± 400	ASTM D 1552
Lower heating value (MJ/kg)	43.34 ± 0.21	42.66 ± 0.20	ASTM D 240
Higher heating value (MJ/kg)	46.20 ± 0.22	45.52 ± 0.22	ASTM D 240
Density at 20°C (kg/dm ³)	0.792	0.860	–
Hydrogen-to-carbon ratio (mol/mol)	1.87	1.87	–

**Figure 3:** Kerosene analysis according to ASTM standard D-2887-08

In a chemical-looping process ilmenite is usually assumed to be oxidized and reduced according to reaction (3).

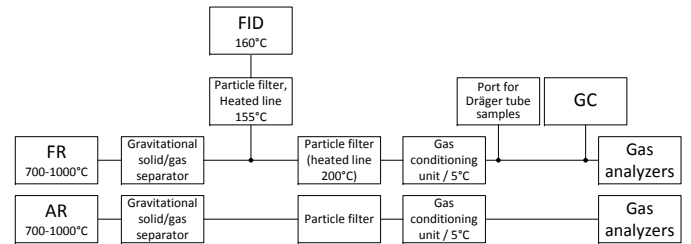


It is known that ilmenite oxygen carrier undergoes structural changes as a consequence of continuous oxidation and reduction. The formation of a separate iron phase and its migration to the particle surface after several redox cycles has been reported in several publications [16–18]. The extent to which the iron migration happens and the number of redox cycles needed seems to depend on how far the oxygen carrier is reduced in the fuel reactor. Ilmenite has been studied in chemical-looping applications with solid fuels [19–22] and gaseous fuels [16, 17, 20, 23, 24]. Compared to synthesized oxygen carriers, ilmenite is cheap, as no production step is needed to obtain the oxygen carrier particles. The ilmenite used here was supplied by Titania A/S, Norway. It was reported 94.3 wt-% pure and had a slight excess of iron, compared to stoichiometric ilmenite. The reactor was filled with about 380 g of ilmenite in the size range of 90–212 μm.

2.5. Measurements

Figure 4 shows a schematic of the gas measurement system. The top parts of the air and fuel reactors are connected to a gravitational solid/gas separator. Part of the hot flue gases of the fuel reactor are diverted and led through a heated line, at 155°C, to a flame ionization detector (FID). The FID measures

the content of organic carbon as CH₄ equivalent, without giving information about the hydrogen content. The flue gases of both air and fuel reactors are separately filtered and cooled down to 5°C, before they pass through gas analyzers. The dry-gas content of CH₄, CO and CO₂ is measured by infrared (IR) analyzers and the content of O₂ by a paramagnetic sensor. Additionally, the dry fuel reactor gas is analyzed with a gas chromatograph (GC), which measures, besides the previously mentioned gases, H₂, N₂, and hydrocarbons up to C₃H₈. The GC used is equipped with two columns, Molsieve MS5Å 10 m × 0.32 mm (ID) and PoraPLOT Q 10 m × 0.15 mm (ID), in which the gas sample is injected in parallel.

**Figure 4:** Schematic measurement layout

When the sulfurous kerosene was used, flue gas from the fuel reactor was kept at about 200°C by means of heated lines and quenched to 5°C in the gas conditioning unit. In this way condensation of steam to water and dissolution of sulfur-species in aqueous phase in the gas line could be reduced. Sulfur species SO₂ and H₂S were measured intermittently using Dräger detector tubes. Such detector tubes contain solid agents for one particular gas and one measuring range. The concentration of the examined gas is indicated colorimetrically, which allows a direct reading. Different detector tubes for SO₂ and H₂S at different measuring ranges were used. The detection limits of SO₂ and H₂S for the detector tubes used was 50 ppmv and 0.2 ppmv respectively. In addition to the detector tube measurements, an SO₂ IR analyzer was connected in series with the IR gas analyzers of either the air reactor or the fuel reactor.

Before and after the experiments, the ilmenite particles were analyzed using SEM/EDX and XRD. The bulk density and the BET surface area (through gas adsorption) of the oxygen carrier particles were also measured before and after the experiments.

2.6. Conducted Experiments and Calculations

This paper presents the results from two series of experiments. During all experiments particles in the air reactor were fluidized with 8 L_n/min air and a total of 0.85 L_n/min argon was added to fluidize the loop-seals. In the injection system 0.93 L_n/min steam were mixed with the different amounts of fuel used.

In the first experimental series, the ilmenite oxygen carrier was used with sulfur-free kerosene. Bed temperatures in the fuel reactor between 750°C and 950°C were investigated and the fuel flow was varied between 0.25 ml_{liq}/min and 1.00 ml_{liq}/min (143–572 W_{th}), which corresponds to hydrogen-to-carbon ratios of 7.7–3.3 as the amount of steam used in the injection system was constant. During this series experiments with addition of sulfur-free kerosene were performed for 41 h.

For the second series of experiments, both sulfur-free and sulfurous kerosene were used as fuel. A set of experiments with sulfurous kerosene was performed between two sets of experiments with sulfur-free kerosene with the purpose to investigate whether the performance of the oxygen carrier changed during exposure to sulfur components. The flow of sulfurous kerosene was varied between 0.164 ml_{liq}/min and 0.654 ml_{liq}/min (100–400 W_{th}), which corresponds to hydrogen-to-carbon ratios of 10.1–3.9. Bed temperatures in the fuel reactor were investigated in the range of 850–950°C. During the second series, 30 h of experiments were performed with addition of sulfurous kerosene and 9 h with sulfur-free kerosene.

Before the first test series was started, the ilmenite oxygen carrier particles were carefully oxidized in air by slowly increasing the temperature and maintaining a fluidized bed regime. Then the batch of oxygen carrier was activated by continuously oxidizing and reducing the particles. Syngas, consisting of 50% H₂ and 50% CO, was used as a reducing agent for 1 h and sulfur-free kerosene for 8 h. The batch of oxygen carrier used for test series 2 consisted of 95% of material from series one and 5% of fresh material.

Thermodynamic equilibrium calculations were performed using Factsage 6.3.1 with the databases FToxid and FTmisc [25].

3. Data Evaluation

3.1. Fuel Conversion

The evaluation of the conversion of carbon uses data from three different analyzers, IR analyzers, GC and FID. Carbon fractions f_{Ci} are calculated, which are the fractions of fuel-C in the fuel reactor converted to CO, CO₂, CH₄ and hydrocarbons higher than CH₄ (C₂ ... C₉). The term "yield" is used for the carbon fraction of CO₂.

$$f_{Ci} = \frac{\dot{n}_{Ci}}{\sum \dot{n}_{Ci,FR,out}} = \frac{y_{Ci}}{y_{CO_2} + y_{CO} + y_{CH_4} + \sum_{m=2}^9 (m \cdot y_{C_mH_n})} \quad (4)$$

The evaluation of the conversion of sulfur is shown as SO₂ yield, based on dry-gas measurements of SO₂ and H₂S with

detector tubes, see Section 2.4.

$$f_{SO_2} = \frac{\dot{n}_{SO_2}}{\dot{n}_{SO_2} + \dot{n}_{H_2S}} = \frac{x_{SO_2}}{x_{SO_2} + x_{H_2S}} \quad (5)$$

3.2. Oxygen Carrier

The actual oxygen carrier reduction can be described through the degree of oxidation, X , see equation (6), and the degree of mass-based conversion, ω , see equation (7). m_{OC} is the actual mass of the oxygen carrier, $m_{OC,red}$ the mass in the most reduced state and $m_{OC,ox}$ the mass in the most oxidized state.

$$X = \frac{m_{OC} - m_{OC,red}}{m_{OC,ox} - m_{OC,red}} \quad (6)$$

$$\omega = \frac{m_{OC}}{m_{OC,ox}} \quad (7)$$

The actual mass of the oxygen carrier, m_{OC} , cannot be determined explicitly during operation of the 300 W reactor. Hence, the only way to ascertain the actual reduction is to indirectly infer it from how much oxygen is needed to oxidize the oxygen carrier after the fuel flow is shut off. This so called reoxidation is usually performed at the end of each experiment.

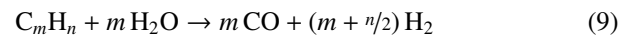
It is possible to calculate the oxygen carrier circulation, \dot{m}_{OC} , see equation (8), as a function of ω and the oxygen consumed in the air reactor, $\Delta\dot{m}_{O_2,AR}$, under the assumption that the oxygen carrier is fully oxidized in the air reactor. Here, ω is derived from reoxidation data, see equation (7), and $\Delta\dot{m}_{O_2,AR}$ from continuous operation. Hence, the oxygen carrier circulation can be estimated for the one air reactor air flow, which was used prior to reoxidation.

$$\dot{m}_{OC} = \frac{\Delta\dot{m}_{O_2,AR}}{1 - \omega} \quad (8)$$

4. Results and Discussion

4.1. Carbon Conversion of Sulfur-free Kerosene (Series 1)

The results of the series with sulfur-free kerosene are shown in Figure 5. One trend that can be observed clearly is that the fraction of C₂ ... C₉ decreases with increasing temperature, while the fraction of CO increases. Hydrocarbon decomposition is known to increase with increasing temperatures. Additionally, the presence of steam, from the injection system and as a product of fuel conversion, triggers steam reforming of hydrocarbon according to reaction (9).



For the fuel flows in Figure 5, the flow of steam in the injection system is above the minimum needed to reform the fuel fully to CO and H₂. The fact that hydrocarbons are detected shows that equilibrium is not reached.

The maximum fuel carbon conversion to CO₂ was about 84% at 900°C and 143 W_{th} fuel equivalent, see Figure 5, of all

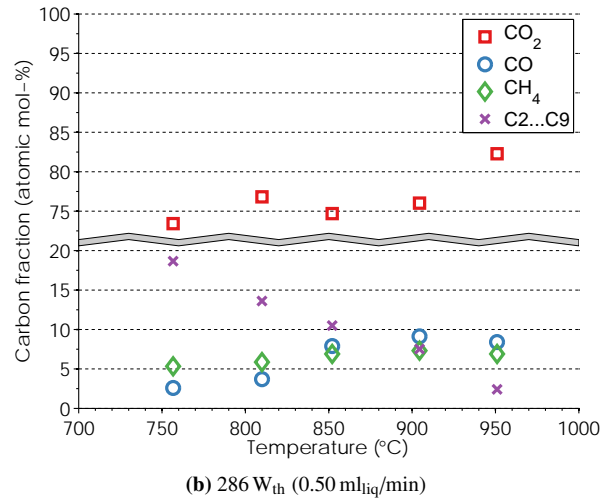
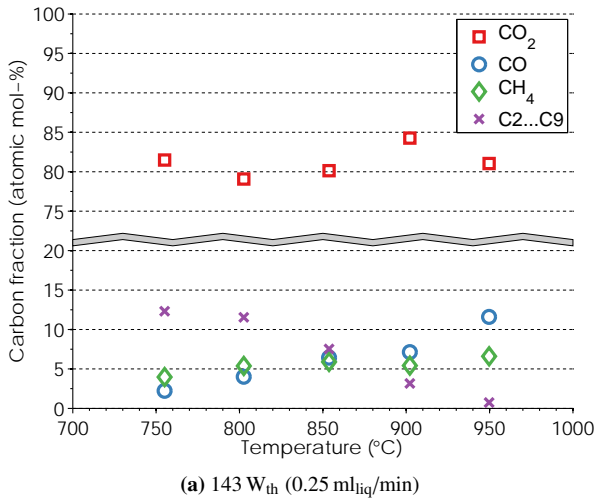


Figure 5: Carbon fractions for different fuel flows of sulfur-free kerosene and different temperatures (series 1)

fuel flows and all temperatures tested in series 1. Whereas the CO_2 yield does not follow a clear trend when the temperature is varied, the overall degree of oxidation of fuel increases with temperature.

The concentrations of CO and H_2 measured increased with temperature. Usually the concentration of H_2 was about twice as high as the concentration of CO. There is a clear increase in the CO concentration in Figure 5a. Prior studies have found that there is an increase in reactivity of CO with ilmenite as a function of temperature [26], and hence the increase is likely associated with the increase in CO and H_2 production from hydrocarbon decomposition, which may take place throughout the bed of particles. Thus some of the gas may have insufficient residence time to react completely.

It can be speculated that the combustion of kerosene in the fuel reactor is a combination of hydrocarbon decomposition, steam reforming, and oxidation of H_2 and CO by the ilmenite particles. Direct oxidation of CH_4 or other hydrocarbons seems less likely.

At the end of each experiment the particles in the fuel reactor were reoxidized to see whether fuel carbon had accumulated in the reactor. The amount of carbon that was released as CO_2 during such reoxidation usually corresponded to less than 0.6% of the total fuel carbon added during the preceding experiment. The carbon is likely formed through decomposition of hydrocarbons on the particle surface.

4.2. Carbon Conversion of Sulfurous Kerosene (Series 2)

Experiment series 2 was commenced using sulfur-free kerosene, see Figure 6a. The results are similar to the ones from series 1, cf. Figure 5a, except at 950°C . The conversion of fuel improved drastically over the experiments with sulfurous fuel, as can be seen by comparing Figures 6a and 6b.

The mechanisms that are discussed in Section 4.1 should also apply when sulfurous kerosene is used, i.e., the trends observed in Figure 5 should be similar to the trends in Figure 7, which shows the results for the experiments with sulfurous

kerosene. This similarity does not appear to be the case. The carbon fractions of CO, CH_4 and other hydrocarbons, $\text{C}_2 \dots \text{C}_9$, decreased somewhat with higher temperatures and the CO_2 yield increased. The concentrations of H_2 and hydrocarbons measured were generally low; below 3% for all fuel flows at 850°C , below 2% for all fuel flows at 900°C and below 1% for all fuel flows at 950°C . This indicates a high conversion to H_2O .

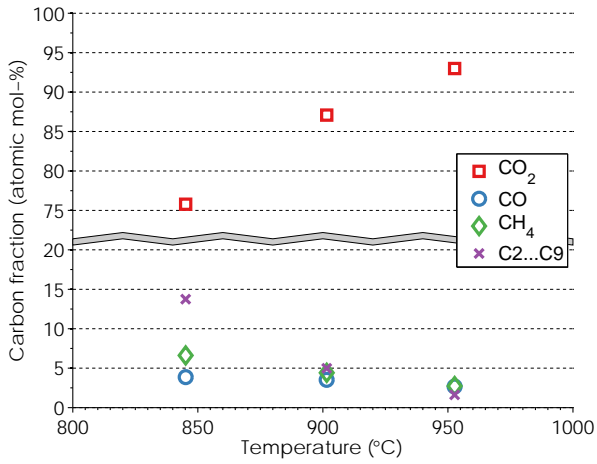
The amount of carbon that was released as CO_2 during reoxidation of particles corresponded to less than 0.8% of the total fuel carbon added during the experiment.

A detailed analysis of the 33 h of operation with and without sulfur was made, clearly indicating that a dramatic increase in reactivity takes place within the first five hours of operation with sulfurous fuel. All periods before these first five hours showed low reactivity, whereas all periods after showed high reactivity, in accordance with the data for $144 \text{ W}_{\text{th}}$ shown in Figure 8 and Table 2.

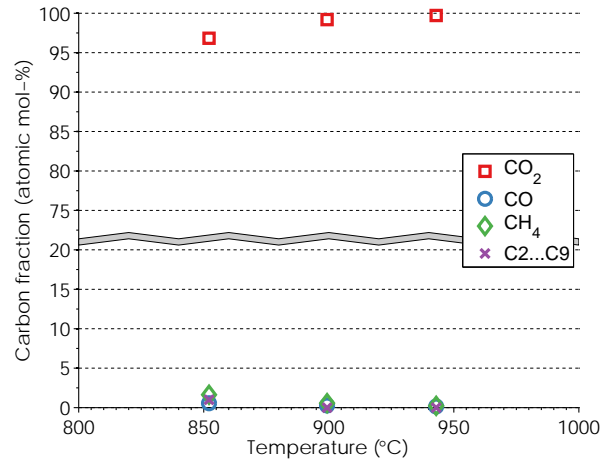
Table 2: Order of experiments in series 2 as indicated in Figure 8

Number of experiment	Cumulative operation time (h)	Fuel reactor temperature ($^\circ\text{C}$)	Type of kerosene
1	0.5	850	
2	1.3	900	sulfur-free
3	1.9	950	
4	2.7	900	
5	9.7	950	sulfurous
6	16.0	850	
7	30.2	850	
8	31.9	900	sulfur-free
9	33.5	950	

A separate analysis was carried out in a batch reactor to investigate the change in reactivity of the ilmenite oxygen carrier particles. Material from the experiments with sulfurous kerosene

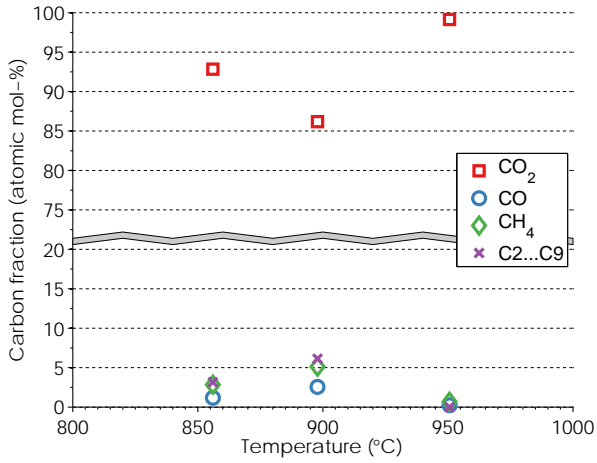


(a) Before experiments with sulfurous kerosene

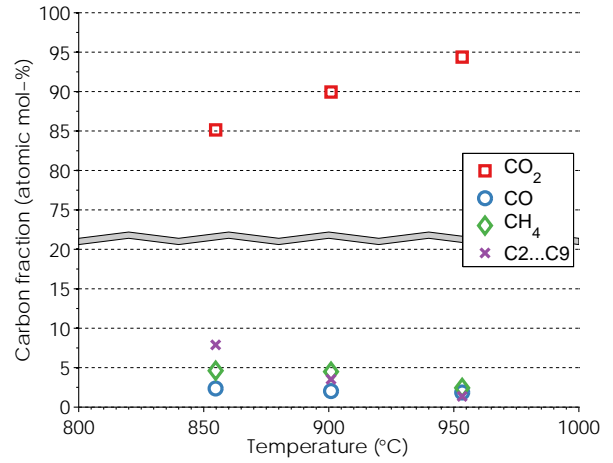


(b) After experiments with sulfurous kerosene

Figure 6: Carbon fractions for 143 W_{th} (0.25 ml_{iq}/min) of sulfur-free kerosene at different temperatures (series 2)



(a) 144 W_{th} (0.236 ml_{iq}/min)



(b) 300 W_{th} (0.492 ml_{iq}/min)

Figure 7: Carbon fractions for different fuel flows of sulfur-free kerosene and different temperatures (series 2)

was compared with freshly activated ilmenite. The activation of ilmenite was carried out in a batch fluidized-bed reactor made of quartz glass and a diameter of 22 mm. 6 g of the ilmenite oxygen carrier were mixed with 9 g of inert quartz sand. At 850–950°C, the particles were alternately oxidized with 10% O₂ in nitrogen and reduced by syngas, containing 50 vol-% CO and 50 vol-% H₂, for a total number of 25 redox cycles. A detailed description of the activation process can be found in [26].

For the reactivity analysis about 6 g of the ilmenite particles were mixed with 9 g of quartz sand, both in the size fraction of 125–180 μm. A detailed scheme of the fluidized-bed setup and reactor dimensions can be found elsewhere [27]. Freshly activated particles and the particles used in this study were reduced with methane at 950°C. The reactor was heated to the set temperature in 10% O₂ in N₂ to ensure full oxidation of the carrier prior to the experiments. The bed was then exposed to alternating oxidizing and reducing conditions to simulate the CLC system. Methane was used for 18 s during the reduction period

and the experiment was repeated for at least three times. Nitrogen was used as an inert purge for 60 s in between oxidation and reduction to avoid the mixing of gases. The inlet flow rate was kept constant at 0.9 L_N/min during reduction, oxidation and inert periods.

Figure 9 shows the conversion of methane to CO₂, the CO₂ yield, as a function of the degree of mass-based conversion of oxygen carrier, ω , see equations (4) and (7). It can be seen that the conversion of the methane is much higher with the used ilmenite than with the freshly activated ilmenite. This confirms that the oxygen carrier material was activated in some way during the experiments with sulfur.

4.3. Sulfur Conversion (Series 2)

The SO₂ yield improved with increasing temperature and decreasing fuel flow, see Figure 10, and thus follows the same trends as the CO₂ yield. The concentration of SO₂ in the air reactor was measured continuously for all fuel flows at 900°C, to

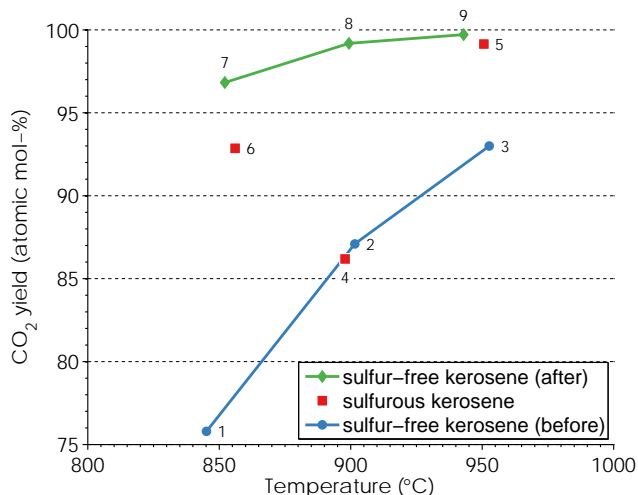


Figure 8: Comparison of experiments with sulfur-free and sulfurous kerosene in series 2. A constant fuel flow equivalent of $144 W_{th}$ was used. The numbering of the points corresponds to the order in which the experiments were performed, cf. Table 2.

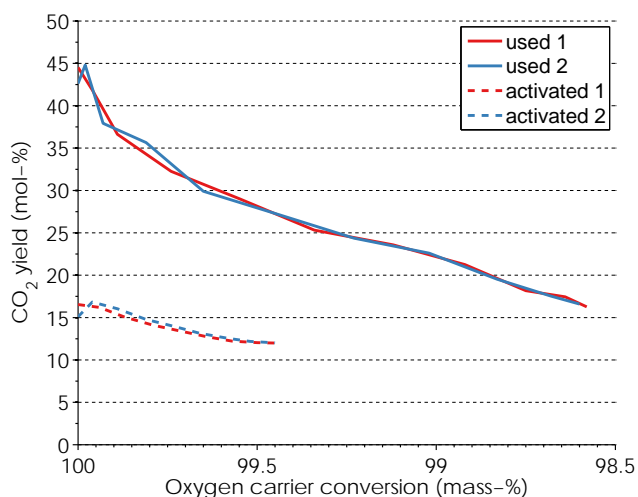


Figure 9: CO_2 yield as a function of mass-based conversion of oxygen carrier. Freshly activated ilmenite oxygen carrier ("activated") is compared with the material used for the experiments with sulfurous kerosene ("used"). Two reductions with methane are plotted for each oxygen carrier.

establish if sulfur could follow the solid circulation to the air reactor and become oxidized there. The concentrations measured were below 200 ppmv, which corresponds to less than 0.4 mol-% of the fuel sulfur. This is less than the carbon leakage to the air reactor.

The sum of H_2S and SO_2 measured after the fuel reactor was typically 20–70% below the expected value. Deposition of sulfur is believed to occur in two places in the system. Firstly, elemental sulfur is formed from H_2S and SO_2 in the flue gases and condensed in the flue gas exhaust pipe. This phenomenon is discussed further later in this section. Secondly, sulfur, mostly SO_2 , was dissolved in liquid water during condensation of steam in the gas conditioning unit. This is a well-known problem for

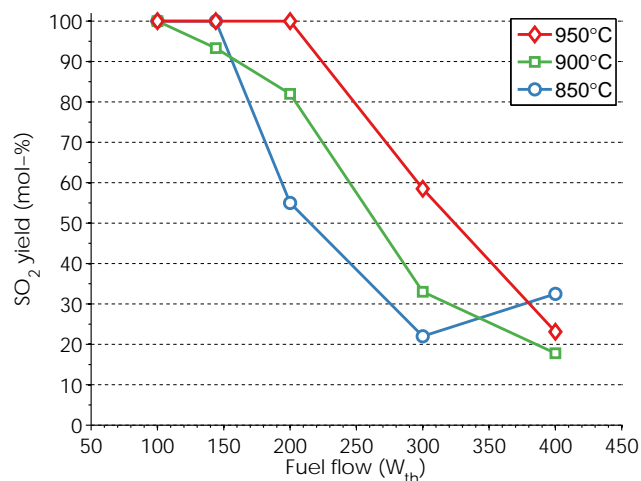


Figure 10: SO_2 yield based on measurements of SO_2 and H_2S for varied fuel flow and varied fuel reactor temperature.

gas measurements at room temperature as were done in this study. A measurement of the pH level of the condensate verified that the condensate was highly acidic, which supports this assumption. The solubility of SO_2 in water is much higher than that of H_2S at conditions similar to those in the gas conditioning unit. It is therefore suspected that the true gradient of the SO_2 yield is much more gradual than the one measured and shown in Figure 10. The trends seem to be correct.

At the end of each experiment the particles in the fuel reactor were reoxidized. After the experiments at $850^\circ C$ a peak of SO_2 from the fuel reactor was observed, which corresponded to 20% of the total fuel sulfur added during the preceding experiment. After the experiments at $950^\circ C$ however, no peak was seen. It seems unlikely that the sulfur accumulated on the particles. Equilibrium calculations were performed with SO_2 and H_2S at different temperatures and it was found that elemental sulfur could be formed at temperatures investigated here, most likely above the bed of the fuel reactor. The reaction mechanism probably corresponds to the Claus process, see reaction (10). Since the amount of H_2S in the flue gases measured depended on the reactor temperature, less elemental sulfur is likely to have formed at $950^\circ C$ than at $850^\circ C$. The sulfur could have condensed in the gas exit pipe of the fuel reactor, where the temperature was kept constant at $400^\circ C$ with an electric heating band. At $400^\circ C$ elemental sulfur in air is oxidized to SO_2 , which happened during the reoxidation of particles in the fuel reactor.



Equilibrium calculations were performed for the gas phase constituents, i.e. C, H, S and O, at the compositions and conditions investigated here. Temperature and oxygen available from the oxygen carrier were varied. Figure 11 shows the results of calculations for $900^\circ C$ as C-, H- and S-fractions at varied amount of oxygen available. It was found that the most important sulfur species are H_2S , at low levels of oxidation, and

SO₂, at high levels of oxidation. COS is only present in minor amounts, about 1 mol-%, at low stoichiometric amounts of oxygen. SO₃ forms first when more oxygen is available than is needed to convert all fuel into CO₂, H₂O and SO₂. In the fuel reactor of a chemical-looping system no free oxygen is available, as the oxygen is bound to the oxygen carrier. Hence, conditions here are always reducing, which makes it unlikely that SO₃ is formed. The degree of oxidation of sulfur could be different for chemical-looping with oxygen uncoupling (CLOU), which is a variation of CLC, where the oxygen carrier releases gas-phase oxygen in the fuel reactor. For more information about CLOU readers are referred to a publication by Rydén et al. [28]. When all fuel is oxidized to CO₂, H₂O and SO₂ and more gas-phase oxygen is available, SO₃ could be formed. This should not be the case for ilmenite though.

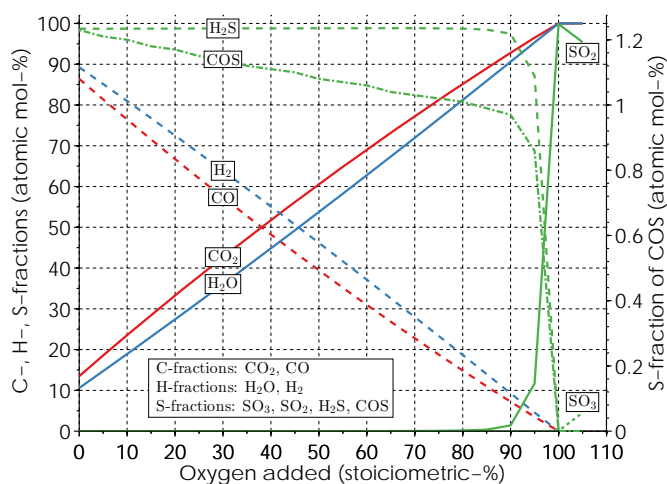


Figure 11: C-, H- and S-fractions of the most relevant species at thermodynamic equilibrium for 900°C with varied amount of oxygen added. The amounts of C, H, S and O correspond to a fuel flow of 300 W_{th} (0.491 ml_{liq}/min) of sulfurous kerosene and 0.75 ml_{liq}/min of steam, as was used in the fuel injection system.

In another equilibrium calculation oxidized ilmenite oxygen carrier was included, i.e., Fe₂TiO₅+TiO₂, and the "free oxygen" was removed. Two cases were evaluated, one with a high oxygen carrier-to-fuel ratio and one where the ratio was very low. Temperatures between 700°C and 1000°C were investigated. In the first case the solid phases formed were pure substances at all temperatures and included TiO₂, Fe₂O₃, Fe₂TiO₅ and Fe₃O₄. No sulfur-containing solid phases were found. The fuel components were nearly fully oxidized, i.e. > 99.9% CO₂, H₂O and SO₂, with some minor amounts of CO and H₂. In the second case different solid solutions were formed that consisted mostly of FeTiO₃ and some Ti₂O₃. At temperatures up to 850°C minor amounts of Fe₃O₄ and FeTi₂O₄ were formed and above 840°C a solid solution was formed that contained elemental sulfur dissolved in elemental iron. The amounts of iron and sulfur were rather low though and corresponded to about 1–3 mol-% of all iron and up to 0.1 mol-% of all sulfur respectively. The fuel components were in the gas phase, which consisted mostly of CO and H₂. Some CO₂ and H₂O were formed and nearly all

sulfur was in the form of H₂S.

It can be concluded that the conversion of sulfur follows that of carbon and that sulfur is unlikely to form on ilmenite oxygen carrier particles at typical chemical-looping conditions.

4.4. Oxygen Carrier Analysis

The XRD analysis of the ilmenite oxygen carrier after series 1 indicated the presence of Fe₂TiO₅ (pseudobrookite), TiO₂ (rutile) and Fe₂O₃ (hematite). This matches earlier findings when syngas was used as fuel [17]. SEM pictures suggest that the phases are not evenly distributed, see Figure 12b, as many particles have elevated spots on their surface. In an EDX analysis of the surface, see Figure 13, it was found that the spots consist mostly of iron and oxygen, possibly Fe₂O₃, and the space in between the spots consists of iron, titanium and oxygen, which could be Fe₂TiO₅ and TiO₂. This differs from the findings made by Adánez et al. [16], where iron oxide formed a continuous shell around a core enriched with titanium. As was pointed out by Cuadrat et al. the extent of the migration of iron phases to the surface of ilmenite oxygen carrier particles seems to depend on how far the oxygen carrier is reduced during operation with fuel [18].

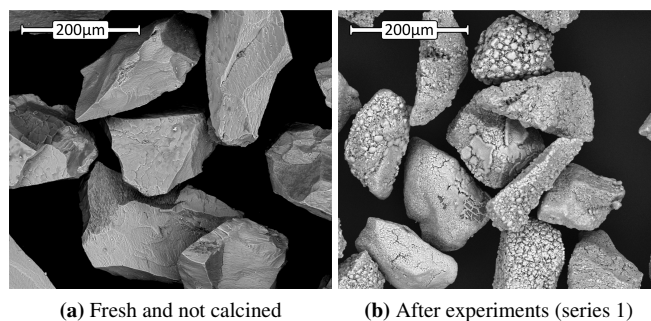


Figure 12: SEM images of ilmenite particles, (a) before, and (b) after experiments with sulfur-free kerosene

After the last experiment of series 2, the oxygen carrier was continuously oxidized and reduced with 400 W_{th} of sulfurous kerosene for about 3 h. The fuel was then replaced with argon, the circulation between air reactor and fuel reactor was stopped and the furnace was switched off. When the reactor had cooled down some of the bed material in fuel reactor was extracted and analyzed with XRD and EDX. Neither analysis showed the presence of sulfur. Hence, it is suspected that the small amount of sulfur, which was detected in the air reactor, cf. Section 4.3, was due to gas leakage and not because of transport with the oxygen carrier particles. It could be speculated that sulfur was formed on the particles, e.g., in the form of S₂, which was oxidized by the oxygen from the oxygen carrier as the particles in the reactor were cooled down in argon. No SO₂ was detected during the cooling down.

The degree of reduction of the oxygen carrier in the fuel reactor and the circulation rates between the air reactor and the fuel reactor were estimated for series 1 and 2. Table 3 shows mean values plus/minus one standard deviation. The results for series 1 and 2 are similar though it appears that circulation was

Table 3: Reduction and circulation of oxygen carrier

Series	Reduction		Circulation	
	ω (%)	X (%)	\dot{m}_{OC} (g/s)	G_{OC}^a (kg/s m ²)
Sulfur-free kerosene (series 1)	98.6 ± 0.7	49.3 ± 23.3	0.65 ± 0.21	10.5 ± 3.4
Sulfurous kerosene (series 2)	97.8 ± 0.4	21.2 ± 15.2	0.98 ± 0.05	15.8 ± 0.8

^a based on the cross-sectional area of the riser section (AR)

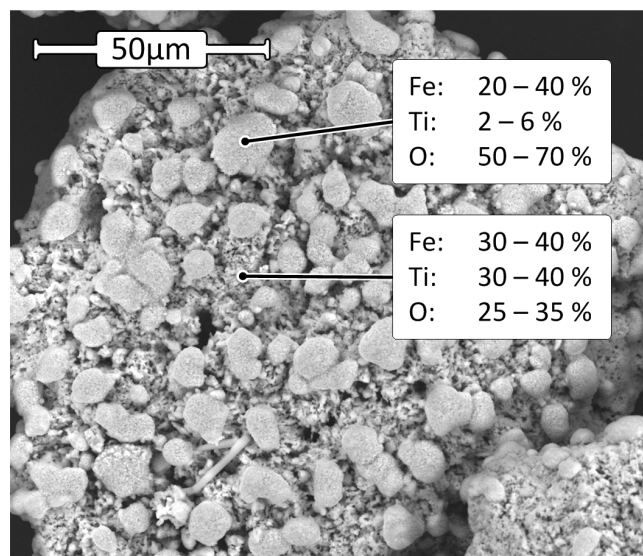


Figure 13: SEM image and results of EDX analysis of ilmenite oxygen carrier after experiments with sulfur-free kerosene (series 1). The indicated phases are shown in molar percent.

slightly higher during series 2. It should be mentioned that the values in Table 3 are based on a limited number of observation only to be able to estimate the order of magnitude of the circulation.

5. Conclusions

- A total of 80 h of fuel operation were performed with sulfurous and sulfur-free kerosene and ilmenite oxygen carrier in a 300 W CLC reactor with continuous circulation of oxygen carrier particles.
- With both types of kerosene CO₂ yields above 99% were reached at 950°C and fuel flows equivalent to 144 W_{th}.
- The presence of sulfur seems to have a positive effect on the reactivity of ilmenite oxygen carrier. Reactivity increased when sulfurous kerosene was used and stayed on a higher level even when sulfur-free kerosene was used thereafter.
- No evidence was found for sulfur poisoning or deactivation of the ilmenite oxygen carrier. Even though possible, it seems unlikely that this should be different for higher concentrations of sulfur.
- More than 99.6 mol-% of the fuel-sulfur left the CLC reactor via the fuel reactor.
- The reactivity of the ilmenite oxygen carrier increased significantly and lasting when sulfurous fuel was used.

- Ilmenite oxygen carrier can be used with sulfurous fuels, both being potentially cheap.

Nomenclature

Symbols

f_{Ci}	(atomic mol-%)	carbon fraction of species i (CO, CO ₂ , CH ₄ and C ₂ ... C ₉)
f_{SO_2}	(mol-%)	SO ₂ yield
G_{OC}	(kg/s m ²)	mass flux of oxygen carrier
$\Delta \dot{m}_{O_2,AR}$	(kg/s)	mass of oxygen consumed in the air reactor
\dot{m}_{OC}	(g/s)	circulation of oxygen carrier
m_{OC}	(kg)	actual mass of oxygen carrier
$m_{OC,red}$	(kg)	mass of oxygen carrier in its most reduced form
$m_{OC,ox}$	(kg)	mass of oxygen carrier in its most oxidized form
$\dot{n}_{Ci,FR,out}$	(mol/s)	molar flow of carbon species i leaving the fuel reactor
\dot{n}_{Ci}	(mol/s)	molar flow of carbon species i
X	(%)	degree of oxidation
x_i	(vol-%)	dry-gas concentration of species i
y_i	(vol-%)	wet-gas concentration of species i
ω	(mass-%)	mass-based conversion of oxygen carrier

Acronyms

AR	air reactor
BET	Brunauer-Emmett-Teller (particle surface area)
CLC	chemical-looping combustion
CLOU	chemical-looping with oxygen uncoupling
EDX	energy dispersive X-ray spectroscopy
FID	flame ionization detector
FR	fuel reactor
GC	gas chromatograph
ID	inner diameter
IR	infrared
OC	oxygen carrier
SEM	scanning electron microscopy
XRD	X-ray powder diffraction

Acknowledgements

The study is carried out under the project "Chemical-looping with liquid hydrocarbon fuels" financed by Saudi Aramco. The authors would also like to thank Harald Jeppsson from Preem

AB for providing the kerosene. Special thanks also to Sven-Ingvar Andersson for conducting fuel analysis and helping with his expertise, to Mehdi Arjmand and Georg Schwebel for conducting the reactivity analysis and to Martin Keller for his help with FactSage.

References

- [1] M. M. Hossain, H. I. de Lasa, Chemical-looping combustion (CLC) for inherent CO₂ separations—a review, *Chemical Engineering Science* 63 (18) (2008) 4433–4451.
- [2] H. Fang, L. Haibin, Z. Zengli, Advancements in Development of Chemical-Looping Combustion: A Review, *International Journal of Chemical Engineering* 2009 (2009) 16.
- [3] A. Lyngfelt, Oxygen carriers for chemical-looping combustion – 4000 h of operational experience, *Oil and Gas Science and Technology* 66 (2) (2011) 161–172.
- [4] J. Adánez, A. Abad, F. García-Labiano, P. Gayán, L. F. de Diego, Progress in chemical-looping combustion and reforming technologies, *Progress in Energy and Combustion Science* 38 (2) (2012) 215–282.
- [5] P. Pimenidou, G. Rickett, V. Dupont, M. Twigg, Chemical looping reforming of waste cooking oil in packed bed reactor, *Bioresource Technology* 101 (16) (2010) 6389–6397.
- [6] P. Pimenidou, G. Rickett, V. Dupont, M. Twigg, High purity H₂ by sorption-enhanced chemical looping reforming of waste cooking oil in a packed bed reactor, *Bioresource Technology* 101 (23) (2010) 9279–9286.
- [7] Y. Cao, B. Lia, H.-Y. Zhao, C.-W. Lin, S. P. Sit, W.-P. Pan, Investigation of Asphalt (Bitumen)-fuelled Chemical Looping Combustion using Durable Copper-based Oxygen Carrier, *Energy Procedia* 4 (2011) 457–464.
- [8] A. Forret, A. Hoteit, T. Gauthier, Chemical Looping Combustion Process applied to liquid fuels, in: *British – French Flame Days*, Lille, France, 37–38, 2009.
- [9] A. Hoteit, A. Forret, W. Pelletant, J. Roesler, T. Gauthier, Chemical Looping Combustion with Different Types of Liquid Fuels, *Oil and Gas Science and Technology* 66 (2) (2011) 193–199.
- [10] T. Mendiara, J. M. Johansen, R. Utrilla, P. Geraldo, A. D. Jensen, P. Glarborg, Evaluation of different oxygen carriers for biomass tar reforming (I): Carbon deposition in experiments with toluene, *Fuel* 90 (3) (2011) 1049–1060.
- [11] A. Lea-Langton, N. Giannakeas, G. Rickett, V. Dupont, M. Twigg, Waste lubricating oil as a source of hydrogen fuel using chemical looping steam reforming, *SAE International Journal of Fuels and Lubricants* 3 (2) (2010) 810–818.
- [12] A. Lea-Langton, R. M. Zin, V. Dupont, M. V. Twigg, Biomass pyrolysis oils for hydrogen production using chemical looping reforming, *International Journal of Hydrogen Energy* 37 (2) (2012) 2037–2043.
- [13] N. Giannakeas, A. Lea-Langton, V. Dupont, M. V. Twigg, Hydrogen from Scrap Tyre Oil via Steam Reforming and Chemical Looping in a Packed Bed Reactor, *Applied Catalysis B: Environmental* 126 (2012) 249–257.
- [14] P. Moldenhauer, M. Rydén, T. Mattisson, A. Lyngfelt, Chemical-looping combustion and chemical-looping reforming of kerosene in a circulating fluidized-bed 300 W laboratory reactor, *International Journal of Greenhouse Gas Control* 9 (2012) 1–9.
- [15] P. Moldenhauer, M. Rydén, T. Mattisson, A. Lyngfelt, Chemical-looping combustion and chemical-looping with oxygen uncoupling of kerosene with Mn- and Cu-based oxygen carriers in a circulating fluidized-bed 300 W laboratory reactor, *Fuel Processing Technology* 104 (2012) 378–389.
- [16] J. Adánez, A. Cuadrat, A. Abad, P. Gayán, L. F. de Diego, F. García-Labiano, Ilmenite activation during consecutive redox cycles in chemical-looping combustion, *Energy and Fuels* 24 (2) (2010) 1402–1413.
- [17] P. Moldenhauer, M. Rydén, A. Lyngfelt, Testing of minerals and industrial by-products as oxygen carriers for chemical-looping combustion in a circulating fluidized-bed 300 W laboratory reactor, *Fuel* 93 (2012) 351–363.
- [18] A. Cuadrat, A. Abad, L. De Diego, F. García-Labiano, P. Gayán, J. Adánez, Prompt considerations on the design of Chemical-Looping Combustion of coal from experimental tests, *Fuel* 97 (2012) 219–232.
- [19] N. Berguerand, A. Lyngfelt, Operation in a 10kW_{th} chemical-looping combustor for solid fuel – Testing with a Mexican petroleum coke, *Energy Procedia* 1 (1) (2009) 407–414.
- [20] E. Jerndal, H. Leion, L. Axelsson, T. Ekvall, M. Hedberg, K. Johansson, M. Källén, R. Svensson, T. Mattisson, A. Lyngfelt, Using low-cost iron-based materials as oxygen carriers for chemical looping combustion, *Oil and Gas Science and Technology* 66 (2) (2011) 235–248.
- [21] C. Linderholm, A. Lyngfelt, A. Cuadrat, E. Jerndal, Chemical-looping combustion of solid fuels – Operation in a 10kW unit with two fuels, above-bed and in-bed fuel feed and two oxygen carriers, manganese ore and ilmenite, *Fuel* 102 (2012) 808–822.
- [22] A. Cuadrat, A. Abad, P. Gayán, L. De Diego, F. García-Labiano, J. Adánez, Theoretical approach on the CLC performance with solid fuels: Optimizing the solids inventory, *Fuel* 97 (2012) 536–551.
- [23] H. Leion, A. Lyngfelt, M. Johansson, E. Jerndal, T. Mattisson, The use of ilmenite as an oxygen carrier in chemical-looping combustion, *Chemical Engineering Research and Design* 86 (2008) 1017–1026.
- [24] H. Leion, T. Mattisson, A. Lyngfelt, Use of Ores and Industrial Products As Oxygen Carriers in Chemical-Looping Combustion, *Energy and Fuels* 23 (2009) 2307–2315.
- [25] Thermfact Ltd., FactSage (version 6.3.1), (software), URL <http://www.factsage.com/>, 2012.
- [26] G. Schwebel, H. Leion, W. Krumm, Comparison of natural ilmenites as oxygen carriers in chemical-looping combustion and influence of water gas shift reaction on gas composition, *Chemical Engineering Research and Design* 90 (9) (2012) 1351–1360.
- [27] M. Arjmand, M. Keller, H. Leion, T. Mattisson, A. Lyngfelt, Oxygen release and oxidation rates of MgAl₂O₄-supported CuO oxygen carrier for chemical-looping combustion with oxygen uncoupling (CLOU), *Energy and Fuels* 26 (11) (2012) 6528–6539.
- [28] M. Rydén, A. Lyngfelt, T. Mattisson, CaMn_{0.875}Ti_{0.125}O₃ as oxygen carrier for chemical-looping combustion with oxygen uncoupling (CLOU)—Experiments in a continuously operating fluidized-bed reactor system, *International Journal of Greenhouse Gas Control* 5 (2) (2011) 356–366.